UCSF

Title

The Hippo Pathway Effector TAZ Regulates Ferroptosis in Renal Cell Carcinoma.

Permalink

https://escholarship.org/uc/item/2bh5g0gd

Journal

Authors

Yang, Wen-Hsuan
Sun, Tianai
Rupprecht, Gabrielle
et al.

Publication Date

DOI

Copyright Information

The Hippo Pathway Effector TAZ Regulates Ferroptosis in Renal Cell Carcinoma

Wen-Hsuan Yang[1,2,3], **Chien-Kuang Cornelia Ding**[1,2], **Tianai Alice Sun**[1,2], **David Shiaowen Hsu**[4], **Jen-Tsan Chi**[1,2,§]

[1]Department of Molecular Genetics and Microbiology, Duke University School of Medicine, Durham, NC 27710, USA

[2]Center for Genomic and Computational Biology, Duke University School of Medicine, Durham, NC 27710, USA

[3]Department of Biochemistry, Duke University School of Medicine, Durham, NC 27710, USA

[4]Department of Medicine, Duke University School of Medicine, Durham, NC 27710, USA

Summary

Despite recent advances, the poor outcomes of renal cell carcinoma (RCC) still necessitate novel therapeutics. RCC is highly susceptible to ferroptosis, a novel form of regulated cell death with disease relevance. While ferroptosis may have therapeutic potential, much remains unknown about the determinants of ferroptosis susceptibility. We found that the ferroptosis susceptibility is highly influenced by cell confluency. RCC grown at low density is highly susceptible to ferroptosis, but exhibits resistance at high density. Because cell density regulates Hippo-YAP/TAZ pathway, we investigated the roles of Hippo pathway effectors in the ferroptosis. TAZ is abundantly expressed in RCC and undergoes density-dependent nuclear/cytosolic translocation. TAZ removal confers ferroptosis resistance, while overexpression TAZS89A sensitizes cells to ferroptosis. Furthermore, TAZ regulates the expression of EMP1 that, in turn, induces the expression of NOX4, a renal-enriched ROS-generating enzyme essential for ferroptosis. Collectively, the cell density-regulated ferroptosis is mediated by TAZ through the regulation of EMP1-NOX4, suggesting its therapeutic potential for RCC and other TAZ-activated tumors.
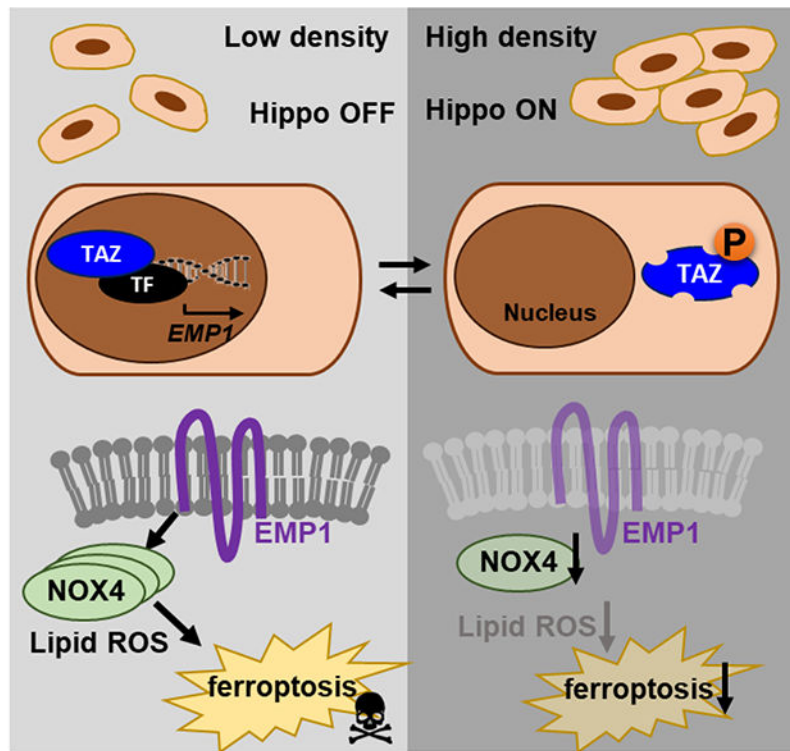
Graphical Abstract

§Corresponding author: Jen-Tsan Chi, jentsan.chi@duke.edu, 101 Science Drive, DUMC 3382, CIEMAS 2177A, Duke Medical School, Durham, North Carolina 27708.

Declaration of Interests

The authors declare no competing interests.

Keywords

Ferroptosis; Renal Cell Carcinoma; Erastin; Hippo pathway; WW Domain Containing Transcription Regulator 1 (TAZ); Epithelial Membrane Protein 1 (EMP1); NADPH Oxidase 4 (NOX4)

Introduction

Renal cell carcinoma (RCC) is the 9th most common cancer in men and 14th in women with approximately 338,000 new cases each year worldwide (Medina-Rico et al., 2018). Despite recent advances in the treatment of RCC using anti-angiogenic agents or immune checkpoint inhibition, the median overall survival rate for patients with the advanced or metastatic RCC remains unsatisfactory (Hsieh et al., 2017). Thus, there is an unmet and urgent need to identify new therapeutic targets and approaches for RCC. RCC cells, among different tumor cells were particular susceptible to ferroptosis, a novel form of iron-dependent programmed cell death (Dixon et al., 2012; Yang et al., 2014), suggesting that inducing ferroptosis may have therapeutic potential for RCC. Ferroptosis is morphologically, genetically, and biochemically different from other cell deaths (Dixon et al., 2012) and characterized by the accumulation of lipid peroxidation products (Yang and Stockwell, 2016). Ferroptosis can be induced by erastin (Dolma et al., 2003), which inhibits the glutamate-cystine antiporter system, xCT, resulting in the redox imbalance by reducing intracellular glutathione levels and accumulation of lipid-based reactive oxygen species (ROS). Lipid ROS can be accumulated by either impaired detoxification of lipid peroxidation via reducing the

expression of glutathione peroxidase 4 (GPX4) (Yang et al., 2014) or by the generation of superoxide and hydrogen peroxide involving upregulation of NADPH oxidases (NOXs) (Dixon et al., 2012). Among different NOXs, NOX4 is highly expressed in the kidney as an important source of renal ROS (Gorin et al., 2005; Sedeek et al., 2013). In addition, inhibition of NOX4 has been reported to reduce the cystine deprivation-induced cell death and lipid ROS, suggesting its essential role in ferroptosis (Poursaitidis et al., 2017). However, much remains unknown about the molecular mechanisms regulating the ferroptosis in RCC to further optimize the therapeutic potential.

In our current study, we show that RCC sensitivity to erastin and ferroptosis is significantly affected by cell density. RCC cells grown under low density were highly susceptible to erastin-induced ferroptosis, while the same RCC cells grown under high confluency become less susceptible to erastin-induced ferroptosis. The Hippo pathway regulators have been established as molecular sensors that regulate density-dependent proliferation of cancer cells (Mori et al., 2014; Zhao et al., 2007). The two Hippo pathway effectors, YAP (Yes Associated Protein 1, encoded by *YAP1*) and TAZ (transcriptional coactivator with PDZ-binding motif, encoded by *WWTR1*), are coactivators of transcription factors primarily through TEAD family proteins, which trigger expressions of genes that determine cell fate and behaviour during embryonic development and oncogenesis. YAP/TAZ activities are regulated by their phosphorylation and intracellular localization. In <u>high</u> cell density, YAP/TAZ are phosphorylated, cytosolically retained and subjected to proteasomal degradation; in <u>low</u> cell density, YAP/TAZ become dephosphorylated and translocate into the nuclei to associate with transcriptional factors to drive gene expression regulating cell proliferation, differentiation and migration (Hsiao et al., 2016; Zhao et al., 2007).

Here, we have established the role of cell density and TAZ in regulating ferroptosis of RCC. In addition, we found that TAZ regulates erastin-induced ferroptosis through the induction of epithelial membrane protein 1 (EMP1), which in turn induces the expression of NADPH oxidase 4 (NOX4) and regulates lipid peroxidation and ferroptosis. Thus, these data support the role of TAZ in regulating ferroptosis through EMP1-NOX4 and that inducing ferroptosis can be a novel therapy for RCC and other TAZ-activated tumors.

Results

Cell density affects the sensitivity of RCC cell lines to erastin-induced ferroptosis

RCCs are susceptible to ferroptosis induced by erastin and cystine deprivation (Tang et al., 2016; Yang et al., 2014). While investigating a renal cancer cell line, RCC4, we observed that the erastin sensitivity was significantly affected by cell density. To characterize this observation further, we systemically examined erastin-induced death of cells grown at different densities. When RCC4 were grown at low cell density (<50% confluency), they were highly sensitive to erastin-induced ferroptosis as the morphologically change of cell rounding shown under light microscopy. In contrast, when the same RCC4 cells were grown at high cell density (>80% confluency), they became significantly less sensitive to erastin (Figure 1A).

Next, the sensitivity of RCC4 to erastin under high and low cell density conditions was quantified by CellTiter-Glo® assay which determined cellular viability using ATP levels (Figure 1B). Cells grown at high density (>80% confluency) was found to be resistant to erastin, whereas cells grown at low density (<50% confluency) were found to be sensitive to erastin. In addition, crystal violet staining also confirmed the reduced erastin sensitivity of RCC4 grown at high cell density (Figure 1C). Similarly, we found cell density-dependent erastin sensitivity in human embryonic kidney cells, 293T (Figure 1D).

The Hippo pathway effectors, YAP/TAZ, mediate cell density-dependent responses (Mori et al., 2014; Zhang et al., 2018; Zhao et al., 2007). Thus, we investigated the role of the YAP/TAZ in the ferroptosis of RCC. First, we determined the expression of YAP and TAZ in two RCC cell lines, RCC4 and 786O. as well as in an early passaged patient-derived xenograft (PDX) RCC cell line, 13-789 (Figure 1I). We found that TAZ, but not YAP, is the predominantly expressed co-activator (Figure 1E). In addition, silencing TAZ in RCC4 and 293T increased the YAP expression, suggesting a compensatory mechanism among the YAP and TAZ (Figure S1A). Therefore, we focused on TAZ as the main effector of the Hippo pathway in RCC cells.

Next, we compared the expression levels of TAZ between cells grown at different density. We found that RCC4 grown at higher cell density expressed a lower level of TAZ protein (Figure 1F), consistent with the cytosolic sequestration and degradation of TAZ during high density (Zhao et al., 2007). In addition, when RCC4 and PDX 13-789 cells were shifted from high density to low density *in vitro*, TAZ translocated from cytosol to nuclei based on immunofluorescence (Figure 1G–H). To verify that the activated TAZ expression in RCC 13-789 PDX tissues also occurred *in vivo*, we performed cytosolic and nuclear fractionations of PDX tissues. As shown in Figure 1I and S1B, the combination of significant nuclear TAZ expression with low level of phosphorylation indicated that TAZ is activated in the RCC 13-789 PDX model. Collectively, these results indicate that TAZ is the predominant Hippo effector in RCC, and its subcellular localization is regulated by cell density.

TAZ regulates sensitivity to erastin-induced ferroptosis

To test the possibility that TAZ regulates cell susceptibility to erastin, we silenced TAZ expression by siRNA and reduced TAZ protein in the RCC4 cell line (Figure 2A). TAZ silencing significantly reduced erastin-induced cell death based on CellTiter-Glo® assay (Figure 2B) and crystal violet staining (Figure 2C). We further find that knockdown of TAZ in the low density RCC4 cells conferred ferroptosis resistance to the similar degrees as high cell density (Figure 2D), suggesting that TAZ activation contributes significantly to the density-dependent ferroptosis sensitivity. In addition, knockdown of TAZ in RCC4 by multiple independent siRNAs all reduced sensitivity to erastin (Figure 2E and S2A). To determine if similar results were observed in other RCC cells, we silenced TAZ expression in both 786O and 13-789 cells. We found that TAZ knockdown also reduced the erastin sensitivity in these cell lines (Figure 2F–G and S2B–C).

Conversely, we tested whether forced activation of TAZ would also affect erastin sensitivities. The expression of a constitutively active form of TAZ, TAZS89A (Lei et al., 2008), significantly increased the sensitivity of RCC4 to erastin (Figure 2H–I). Collectively,

these data strongly indicate that the activation status of TAZ regulates the sensitivities to erastin-induced ferroptosis under different cell density.

EMP1 is a direct target gene of TAZ that regulates ferroptosis sensitivity

Next, we sought to identify the mechanism by which TAZ regulates erastin sensitivity in the RCC4 cell line. TAZ is a transcriptional-coactivator which affects cellular phenotypes through transcriptional regulation of its target genes. Based on the assumption that TAZ silencing may repress genes essential for ferroptosis, we focused on genes which were both repressed during TAZ knockdown and essential for the cystine-deprived death of RCC4 (RNAi screen). To accomplish this, we determined the global gene expression response to knockdown of TAZ in RCC4 and integrated these affected genes with a previously completed genome-wide RNAi screen under cystine deprivation (manuscript in preparation). RNA was isolated from RCC4 transfected with either control (siNT) or TAZ-targeting siRNAs (siTAZ) with or without erastin treatment in triplicates (Figure S3A) and hybridized to Affymetrix U133A2.0 microarrays (Figure 3A). The transcriptional responses of the TAZ knockdown were then derived by zero-transformation against the average of the DMSO-treated siNT control samples as previously performed (Keenan et al., 2015; Tang et al., 2017). Next, we identified the candidate genes which were both repressed during TAZ knockdown (microarrays) and found to be essential for the cystine-deprived death of RCC4 (RNAi screen) (Figure S3B). From these comparisons, we identified eleven candidate genes, including TAZ. After excluding TAZ and two other genes encoding only one subunit of multi-component protein complexes, we set up a mini-screen to prioritize the eight remaining candidate genes. First, we used qRT-PCR to validate the mRNA downregulation upon TAZ removal (Figure S3C). Second, we performed functional assays to determine if each candidate gene was essential for ferroptosis in RCC4 (Figure S3D). Based on these criteria, the epithelial membrane protein 1 (EMP1) emerged as the most promising candidate. The EMP1 mRNA was significantly down-regulated upon TAZ silencing (Figure 3B). In addition, we found that EMP1 silencing by multiple siRNAs protected RCC4 from erastin-induced death (Figure 3C and S3E). EMP1 knockdown also conferred ferroptosis resistance in 786O cells (Figure 3D and S3F). Therefore, the downregulation of EMP1 may contribute to the ferroptosis resistance conferred by the TAZ silencing.

Next, we examined whether overexpression of EMP1 may sensitize ferroptosis after TAZ knockdown. First, we observed that overexpression of V5-tag EMP1 significantly sensitized RCC4 to erastin (Figure 3E and S3G). Next, RCC4 stably expressing control vector (pLX304) or V5-tag EMP1 were transfected with either control (siNT) or TAZ-targeting siRNAs (siTAZ) followed by erastin treatment. Overexpression of EMP1 significantly reduced the ferroptosis protection conferred by TAZ knockdown (Figure 3F). This is consistent with the concept that the repression of EMP1 genetically works downstream of TAZ to regulate ferroptosis.

Previous ChIP-seq studies have indicated that the regulatory regions of EMP1 were physically associated with YAP/TAZ/TEAD complexes (Stein et al., 2015; Walko et al., 2017; Zanconato et al., 2015). To validate that EMP1 is a direct target gene of TAZ, we performed ChIP-qPCR using an antibody specific for endogenous TAZ protein. As shown

in Figure 3G, we found that a well-known YAP/TAZ target gene, connective tissue growth factor (CTGF), was highly enriched in the TAZ pull-down (Figure 3G). Similarly, EMP1 was also significantly enriched in the TAZ pull-down, indicating that EMP1 promoter is directly associated with TAZ. Together, these data support the binding of TAZ to the promoter of EMP1 as a potential direct target gene and its downregulation upon TAZ silencing contributes to the ferroptosis resistance phenotypes.

EMP1 regulates ferroptosis through NOX4

To investigate the mechanistic link between EMP1 and ferroptosis, we sought to determine whether EMP1 would affect the levels of GPX4 or NOX4, two key regulators of lipid peroxidation and ferroptosis (Dixon et al., 2012; Poursaitidis et al., 2017; Yang et al., 2014). We found that EMP1 silencing decreases the mRNA expression of NOX4, but not GPX4 (Figure 4A and S4A–B). Conversely, overexpression of EMP1 increases the mRNA level of NOX4, but not GPX4 (Figure 4B and S4C–D). Consistently, overexpression of EMP1 also increases NOX4 protein level (Figure 4C), but not GPX4 protein level (Figure S4E). Thus, we reasoned that EMP1 may regulate ferroptosis through affecting the levels and activities of NOX4. Consistent with its ability of to induce EMP1, TAZS89A also increased the level of NOX4 protein (Figure S4F), but not GPX4 (Figure S4E). Furthermore, NOX1/NOX4 inhibitor, GKT136901 (Laleu et al., 2010) protected RCC4 from ferroptosis (Figure 4D). Since NOX1 was not expressed at detectable levels in RCC cell lines (Gregg et al., 2014), GKT136901 probably mediated the ferroptosis protection through NOX4. Consistently, silencing of NOX4 by siRNAs also conferred ferroptosis resistance (Figure 4E and S4G). To investigate the genetic interaction between EMP1 and NOX4, we treated the NOX4 inhibitor, GKT136901, in EMP1-overexpressing RCC4. We found that the EMP1 overexpression increased erastin sensitivity, but this increased sensitivity was abolished by GKT136901 (Figure 4F).

In addition, as p38 MAPK has been reported to regulate NOX4 reciprocally (Dougherty et al., 2017; Huang et al., 2018; Park et al., 2010; Peng et al., 2013), we examined the role of p38 activity in the NOX4 induction by EMP1. We found that EMP1 expression increase the phosphorylation and activation of p38 (Figure 4G). Furthermore, EMP1 silencing reduced the p38 phosphorylation (Figure 4H). In addition, p38 inhibitor, SB203580, abrogated the increase of NOX4 associated with EMP1 expression (Figure 4I).

Finally, because the accumulation of lipid-based reactive oxygen species (lipid ROS) is crucial for ferroptosis (Dixon et al., 2012), we measured the lipid ROS by C11-BODIPY staining combined with flow cytometry detection. As shown in Figure 4J and S4H, the increased accumulation of lipid ROS induced by erastin is abolished by knockdown of TAZ or knockdown of EMP1 as well as NOX4 inhibitor, GKT136901. Taken together, we propose a signaling mechanism (Figure 4K), in which TAZ is a cell-density-dependent determinant of ferroptosis sensitivity through affecting the levels EMP1, which in turn regulates NOX4, lipid peroxidation and ferroptotic death of RCC.

Discussion

Here, we provide evidence that a non-genetic factor, cell density, contributes to the regulation of ferroptosis sensitivities. Similar observation is also reported in a preprint on BioRxiv (Panzilius et al., 2018). Importantly, we have elucidated a molecular mechanism by which cell density regulates ferroptosis in RCC through the Hippo pathway effector, TAZ, which affects the levels of EMP1, NOX4 and lipid peroxidation. As the Hippo pathway and YAP/TAZ has been implicated in sensing cell density, the activation status of TAZ contributes significantly to density-dependent ferroptosis. Furthermore, we found that TAZ directly binds to the EMP1 promoter region and regulates the EMP1 expression. The higher EMP1 protein, in turns, regulates ferroptosis through elevating NOX4 and resulting lipid peroxidation. Higher levels of NOX4 has been reported to enhance lipid peroxidation and sensitize cells to ferroptosis (Poursaitidis et al., 2017). Consistent with our findings, sub-confluent colonic epithelial cells have higher ROS production than cells in confluent cells (Perner et al., 2003). Collectively, our results suggest that TAZ activation may sensitize cells to ferroptosis and be predictive of sensitivity to ferroptosis-inducing agents.

YAP/TAZ and other components of the Hippo pathway integrate a wide variety of non-genetic factors, such as cell density, mechanical properties and metabolic status (Zanconato et al., 2016). Therefore, the regulation of ferroptosis susceptibility by TAZ suggests that these non-genetic factors may play important roles in ferroptosis sensitivities. For example, both epithelial-mesenchymal transition and fibrosis are prominent features of RCC. These changes may create the "stiff" extracellular environment known to activate the YAP/TAZ, which may promote the sensitivities to ferroptosis. In addition, YAP/TAZ is also regulated by metabolic pathways. A previous study has shown the essential role of glutamine metabolism in ferroptosis (Gao et al., 2015) but the mechanisms remain unclear. YAP/TAZ has been reported to be activated by O-GlcNAcylation (Peng et al., 2017), a reversible modification that is highly sensitive to glucose or glutamine levels (Chen et al., 2018; Chen et al., 2017). Therefore, it is tempting to hypothesize that nutrient-sensing O-GlcNAcylation of YAP/TAZ may contribute to the metabolic regulation of ferroptosis by glutamine metabolisms.

Several studies have implicated Hippo pathways in various types of RCC (Cao et al., 2014; Schutte et al., 2014; Sourbier et al., 2018). However, most of these papers have focused on the expression and role of YAP without rigorously testing the expression and function of TAZ. Our results suggest the expression and functional role of TAZ in the RCC cell lines and early passage tumor cells. In addition, YAP can be induced in RCC4 upon TAZ silencing. Therefore, it will be important to clearly distinguish between these two highly similar but distinct Hippo effectors, especially when some detection reagents and methods may not reliably distinguish between YAP and TAZ.

Our results may also have significant therapeutic implications. While inducing ferroptosis may have significant anti-tumor potential, much remains unknown to select tumors which may best respond to these ferroptosis-inducing agents. Our results may suggest that TAZ-activated tumors may be particularly responsive to ferroptosis-inducing therapies. In addition, while many tumor cells initially respond to various therapeutic agents, chemo-

resistant persister cells eventually emerge and cause significant morbidity and mortality. Recently, these persister tumor cells are found to express high level of GPX4 and be highly sensitive to ferroptosis (Hangauer et al., 2017; Viswanathan et al., 2017). The drug resistance and persister cells are also known to be associated with YAP/TAZ activation (Lin et al., 2015; Zanconato et al., 2016) and EMP1 expression (Jain et al., 2005). Our results suggest that a GPX4-independent link between chemo-resistance and ferroptosis through TAZ-EMP1-NOX4 activation. Therefore, TAZ-EMP1-NOX4 and ZEB-GPX4 may represent two distinct and independent pathway linking the chemo-resistance with ferroptosis, a possibility that needs to rigorously tested in a large panel of drug-resistant persister cells.

Besides cancer, ferroptosis also has emerging roles in other pathophysiological processes and human diseases, such as neurotoxicity (Skouta et al., 2014), acute renal failure (Angeli et al., 2014), cardiac injury (Gao et al., 2015) and ischemia-reperfusion injury (Linkermann et al., 2014). Therefore, modulating ferroptosis may have therapeutic potentials. In addition, the ability of NOX4 inhibitors to abolish ferroptosis suggests the potential for developing combinational therapies. Currently, several oral NOX4 inhibitors are under preclinical studies (Borbély et al., 2010) and may be tested for their efficacy in mitigating these ferroptosis-associated diseases.

Materials and Methods

Materials and reagents

Erastin was obtained from Duke University Small Molecule Synthesis Facility. The following antibodies were used in this study: YAP/TAZ (#8418, Cell Signaling Technology), phosphor-YAP/TAZ (S127/S89) (#4911, Cell Signaling Technology), beta-actin (sc-130301, Santa Cruz), beta-tubulin (#86298, Cell Signaling Technology), V5-tag (MA5-15253, ThermoFisher Scientific), NOX4 (ab133303, abcam), GPX4 (ab125066, abcam). Horseradish peroxidase (HRP)-labeled goat secondary antibody conjugates were purchased from Cell Signaling Technology. Plasmids are obtained from Addgene (TAZS89A #52084; pLX304 #25890) and DNASU (EMP1 #HsCD00442695).

Cell culture and transfection

RCC cell lines (RCC4 and 786O) were kind gifts from Dr. Denise Chan (Department of Radiation Oncology, University of California, San Francisco), which were further authenticated by DDC (DNA Diagnostics Center) Medical using the short tandem repeat method in November 2015. HEK-293T was acquired from the Duke Cell Culture Facility. All cells are cultured in Dulbecco's Modified Eagle Medium (11995-DMEM, ThermoFisher Scientific) with 10% heat-inactivated Fetal Bovine Serum (HyClone™ FBS, GE Healthcare Life Sciences #SH30070.03HI) in a humidified incubator at 37°C and 5% CO_2. Transfections were performed according to the manufacturer's instructions with TransIT-LT1 transfection reagent (Mirus Bio) or RNAiMax transfection reagent (ThermoFisher Scientific).

siRNA-mediated gene knockdown

All human siRNAs were purchased from Dharmacon or Qiagen: Non-targeting control, siNT (Qiagen SI03650318); siTAZ (Dharmacon M-016083-00); siYAP (Dharmacon M-012200-00); siEMP1 (Dharmacon M-010507-00); siNOX4 (Dharmacon M-010194-00); siANGPTL4 (Dharmacon M-007807-02); siGPSM3 (Dharmacon M-013906-00); siSGPL1 (Dharmacon M-008747-00); siSMAGP (Dharmacon M-015427-01); siSMG5 (Dharmacon M-014023-00); siTAZ#1 (Qiagen SI00111230); siTAZ#2 (Qiagen SI00111237); siTAZ#3 (Qiagen SI00111216); siTAZ #4 (Dharmacon D-016083-01); siTAZ #5 (Dharmacon D-016083-02); siEMP1#1 (Dharmacon D-010507-02); siEMP1#2 (Qiagen SI04260711); siTAZ#3 (Qiagen SI04327862); siTAZ #4 (Dharmacon D-010507-04). siNOX4#1 (Qiagen SI02642500); siNOX#2 (Qiagen SI02642507). The knockdown efficacies were validated by RT-qPCR and/or western blots.

Cell viability assays

After the cells were seeding at the ratio of 2500 cells per 96 well and transfected with siRNAs for 2 days, they are further treated with erastin for additional 24 h. Cell viability was evaluated using the crystal violet staining or the CellTiterGlo™ Luminescent Cell Viability Assay Kit (Promega) according to the manufacturer's instructions. The CellTiterGlo™ Luminescent Cell Viability Assay is based on quantitation of the ATP present indicating metabolically active cells to determine the number of living cells in the culture.

Western blot analysis

For immunoblotting, cells were washed with ice-cold phosphate-buffered saline (PBS), lysed in RIPA buffer (Sigma), supplemented with protease inhibitor (Roche) and PhosSTOP phosphatase inhibitor cocktail (Roche). Proteins were quantified by BCA protein assay (ThermoFisher Scientific). Equal amounts of proteins were resolved by sodium dodecyl sulfate–polyacrylamide gel electrophoresis (SDS-PAGE) and transferred to the polyvinylidene difluoride (PVDF) membrane (Millipore). The membranes were blocked with 5% non-fat milk or BSA, and then probed with indicated antibodies following by HRP-conjugated secondary antibodies. The immuno-signals were achieved by the Amersham ECL prime western blotting detection reagent (GE Healthcare Life Sciences RPN2232) and detected by a Bio-Rad ChemiDoc™ Imaging System.

RNA isolation and quantitative real -time PCR

Total RNAs of culture cells were extracted by using the RNeasy Mini Kit (Qiagen #74104) with DNase I treatment (Qiagen #79254) and the cDNAs were synthesized from 1μg of the RNA template using Superscript™ II Reverse Transcriptase (ThermoFisher Scientific #18064) with random hexamers following protocols from the manufactures. The levels of gene expression were measured by quantitative PCR (qPCR) with Power SYBR Green PCR Mix (Applied Biosystems, ThermoFisher Scientific).

β-actin-F': GGGGTGTTGAAGGTCTCAAA; β-actin-R': GGCATCCTCACCCTGAAGTA; TAZ-F': TGCTACAGTGTCCCCACAAC; TAZ-R': GAAACGGGTCTGTTGGGGAT; YAP-F': CAACTCCAACCAGCAGCAAC; YAP-R': TTGGTAACTGGCTACGCAGG; EMP1-F': GTGCTGGCTGTGCATTCTTG; EMP1-R': CCGTGGTGATACTGCGTTCC;

NOX4-F': CAGATGTTGGGGGCTAGGATTG; NOX4-R': GAGTGTTCGGCACATGGGTA; GPX4-F': GAGGCAAGACCGAAGTAAACTAC; GPX4-R': CCGAACTGGTTACACGGGAA.

Microarray

RCC4 cells exposed to knockdown control, siNT, or knockdown TAZ, siTAZ for two days and then treated with 1 μM erastin for 7 hours. RNAs were extracted by RNeasy Kit (Qiagen), labeled, and hybridized to Affymetrix U133A 2.0 arrays. The microarray data have been deposited into NCBI GEO with accession number: GSE121689 (cDNA microarray for siTAZ). The intensities of Affymetrix probes were normalized by Robust Multi-array Average (RMA) method and zero transformation ($\log_2$) against the control group, siNT (DMSO). Then, the probe sets that varied by $2^{0.8}$-fold in at least two samples were selected for hierarchical clustering.

Generation of Patient-Derived Xenograft (PDX) and Cell lines

Renal cell carcinoma (RCC) tissue sample (13-789) was collected under a Duke IRB-approved protocol (Pro000022289) and all participants provided written informed consent to participate in the study. The patient-derived xenograft (PDX) model of 13-789 was then generated as described previously (Kim et al., 2012; Uronis et al., 2012), and the *in vivo* PDX generation was performed in accordance with the animal guidelines and with the approval of the Institutional Animal Care and Use Committee (IACUC) at the Duke University Medical Center. Briefly, to generate PDXs, the tissue sample was washed in phosphate-buffered saline (PBS), dissected into small pieces (<2 mm), and injected into the flanks of 8-10-week-old JAX NOD.CB17-PrkdcSCID-J mice obtained from the Duke University Rodent Genetic and Breeding Core.

The matched PDX cell line (13-789) was then generated from the PDX as follows. Once the PDX tumors reached a size of >1000 mm^3, tumors were harvested, homogenized and grown in 10 cm^2 tissue culture-treated dishes in cell culture media (DMEM media, 10% fetal bovine serum (FBS), 10 U/ml penicillin and streptomycin) at 37°C and 5% CO$_2$. Clonal populations of each cell line were then obtained by isolating a single clone using trypsinization of the clone sealed off from the dish by an O ring. Finally, the 13-789 cell line was authenticated using the Duke University DNA Analysis Facility Human cell line authentication (CLA) service by analyzing DNA samples from each individual cell line for polymorphic short tandem repeat (STR) markers using the GenePrint 10 kit from Promega (Madison, WI, USA).

Immunofluorescence staining

Cells were cultured on chamber slide (ThermoFisher Scientific #177437) to appropriate density. Cells were fixed with 4% formaldehyde for 10 min and then wash three times with PBS. After blocking in 5% BSA and permeabilized with 0.1% Saponin for 1 hour, slides were incubated with the TAZ antibody (BD Biosciences #560235) 1:100 diluted in 1% BSA with 0.1% Saponin overnight. After washing with PBS, slides were incubated with Alexa Fluor 488-conjugated secondary antibodies (1:200 dilution, ThermoFisher Scientific #A11001) and Alexa Fluor 568-conjugated phalloidin (ThermoFisher Scientific #A12380)

for 1 hour. The slides were then washed and mounted with SlowFade Glod antifade mountant with DAPI ((ThermoFisher Scientific #S36938). Images were acquired using a Leica TCS SP8 confocal microscope equipped with a 40X objective.

ChIP analysis

ChIP-qPCR experiment was carried out according to Myers Lab ChIP-seq protocol. Briefly, RCC4 cells were incubated in cross-linking solution (1% formaldehyde) at room temperature for 10 min and then added 0.125M final concentration of glycine to stop cross-linking. The cells were then washed with cold PBS and suspended in Farnham lysis buffer (5mM PIPES pH8.0, 85mM KCl and 0.5% NP-40) with freshly added protease inhibitor. The lysate was subsequently passed through a 20-gauge needle 20 times to breaks cells while keeping intact nuclei. After centrifugation, the pellet was resuspended with RIPA buffer with freshly added protease inhibitor. Chromatin fragmentation was performed by sonication using the Bioruptor (Diagenode) high speed for 30 min (30 seconds ON, 30 seconds OFF). Proteins were immunoprecipitated in PBS/BSA buffer using TAZ antibody (Cell signaling #70148) or control antibody, rabbit IgG (Cell signaling #2729) which have been conjugated to Dynabeads™ protein G magnetic beads (Thermo Fisher Scientific #10004D) at 4°C for 2 hr. The antibody-chromatin complexes were washed with LiCl wash buffer for 5 times and then washed with TE buffer. The crosslinking was reversed by incubation with elution buffer (1%SDS, 0.1M $NaHCO_3$) at 65°C overnight followed by incubated with RNase A and proteinase K. DNA was recovered by using QIAquick PCR purification kit (Qiagen #28104). Precipitated DNA was analyzed by qPCR using primers targeting TEAD-binding sites found in CTGF (Stein et al., 2015) and EMP1 promoter regions as well as negative control chromatin 14 (Stein et al., 2015). Primer sequences are listed below.

CTGF-F GCCAATGAGCTGAATGGAGT; CTGF-R CAATCCGGTGTGAGTTGATG
EMP1-F TTTGGTGAGGAGGAATGGGC; EMP1-R CAGTCAAGAGTGGCTGGGAG
Ch14-F GTGGGCCTTTGGAATATCCT; Ch14-R GACCTTGGCTGTGTTGTCCT

Lipid ROS assay using flow cytometry

Lipid ROS levels were determined using 10 μM of C11-BODIPY dye (D3861, ThermoFisher Scientific) with positive control, cumene hydroperoxide, according to the manufacturer's instructions. Cells were seeded and treated with siRNAs in six-well plates for two days, then the culture medium was replaced with 1μM erastin treatment for overnight. The next day, the medium was replaced with 10 μM C11-BODIPY-containing medium for 1 hour. Later, the cells were harvested by trypsin and washed three times with ice-cold PBS followed by re-suspending in PBS plus 1% BSA. The amount of ROS within cells was examined by flow cytometry analysis (FACSCanto™ II, BD Biosciences).

Statistical Analyses

Graphs were drawn with GraphPad Prism Software and the statistical analyses were performed using either GraphPad or Microsoft Excel software packages. Data were analyzed using the unpaired Student's t test and expressed as mean ± SEM. P values less than 0.05 were considered significant (*< 0.05; **<0.01; ***<0.001).

Supplementary Material

Refer to Web version on PubMed Central for supplementary material.

Acknowledgement

References

Angeli JPF, Schneider M, Proneth B, Tyurina YY, Tyurin VA, Hammond VJ, Herbach N, Aichler M, Walch A, and Eggenhofer E (2014). Inactivation of the ferroptosis regulator Gpx4 triggers acute renal failure in mice. Nature cell biology 16, 1180. [PubMed: 25402683]

Borbély G, Szabadkai I, Horváth Z, Markó P, Varga Z, Breza N, Baska F, Vántus T, Huszár M, Geiszt M, et al. (2010). Small-Molecule Inhibitors of NADPH Oxidase 4. Journal of Medicinal Chemistry 53, 6758–6762. [PubMed: 20731357]

Cao JJ, Zhao XM, Wang DL, Chen KH, Sheng X, Li WB, Li MC, Liu WJ, and He J (2014). YAP is overexpressed in clear cell renal cell carcinoma and its knockdown reduces cell proliferation and induces cell cycle arrest and apoptosis. Oncol Rep 32, 1594–1600. [PubMed: 25175178]

Chen PH, Chi JT, and Boyce M (2018). Functional crosstalk among oxidative stress and O-GlcNAc signaling pathways: Abstract. Glycobiology.

Chen PH, Smith TJ, Wu J, Siesser PF, Bisnett BJ, Khan F, Hogue M, Soderblom E, Tang F, Marks JR, et al. (2017). Glycosylation of KEAP1 links nutrient sensing to redox stress signaling. EMBO J 36, 2233–2250. [PubMed: 28663241]

Dixon SJ, Lemberg KM, Lamprecht MR, Skouta R, Zaitsev EM, Gleason CE, Patel DN, Bauer AJ, Cantley AM, Yang WS, et al. (2012). Ferroptosis: an iron-dependent form of nonapoptotic cell death. Cell 149, 1060–1072. [PubMed: 22632970]

Dolma S, Lessnick SL, Hahn WC, and Stockwell BR (2003). Identification of genotype-selective antitumor agents using synthetic lethal chemical screening in engineered human tumor cells. Cancer Cell 3, 285–296. [PubMed: 12676586]

Dougherty JA, Kilbane Myers J, Khan M, Angelos MG, and Chen C-A (2017). Dual-specificity phosphatase 4 overexpression in cells prevents hypoxia/reoxygenation-induced apoptosis via the upregulation of eNOS. Frontiers in cardiovascular medicine 4, 22. [PubMed: 28484701]

Gao M, Monian P, Quadri N, Ramasamy R, and Jiang X (2015). Glutaminolysis and transferrin regulate ferroptosis. Molecular cell 59, 298–308. [PubMed: 26166707]

Gorin Y, Block K, Hernandez J, Bhandari B, Wagner B, Barnes JL, and Abboud HE (2005). Nox4 NAD(P)H oxidase mediates hypertrophy and fibronectin expression in the diabetic kidney. J Biol Chem 280, 39616–39626. [PubMed: 16135519]

Gregg JL, Turner RM, Chang G, Joshi D, Zhan Y, Chen L, and Maranchie JK (2014). NADPH Oxidase NOX4 Supports Renal Tumorigenesis by Promoting the Expression and Nuclear Accumulation of HIF2α. Cancer research 74, 3501–3511. [PubMed: 24755467]

Hangauer MJ, Viswanathan VS, Ryan MJ, Bole D, Eaton JK, Matov A, Galeas J, Dhruv HD, Berens ME, Schreiber SL, et al. (2017). Drug-tolerant persister cancer cells are vulnerable to GPX4 inhibition. Nature 551, 247–250. [PubMed: 29088702]

Hsiao C, Lampe M, Nillasithanukroh S, Han W, Lian X, and Palecek SP (2016). Human pluripotent stem cell culture density modulates YAP signaling. Biotechnology Journal 11, 662–675. [PubMed: 26766309]

Hsieh JJ, Purdue MP, Signoretti S, Swanton C, Albiges L, Schmidinger M, Heng DY, Larkin J, and Ficarra V (2017). Renal cell carcinoma. Nature Reviews Disease Primers 3, 17009.

Huang Y, Cai G.-q., Peng J-P, and Shen C (2018). Glucocorticoids induce apoptosis and matrix metalloproteinase-13 expression in chondrocytes through the NOX4/ROS/p38 MAPK pathway. The Journal of steroid biochemistry and molecular biology 181, 52–62. [PubMed: 29526705]

Jain A, Tindell CA, Laux I, Hunter JB, Curran J, Galkin A, Afar DE, Aronson N, Shak S, Natale RB, et al. (2005). Epithelial membrane protein-1 is a biomarker of gefitinib resistance. Proceedings of the National Academy of Sciences of the United States of America 102, 11858–11863. [PubMed: 16087880]

Keenan MM, Liu B, Tang X, Wu J, Cyr D, Stevens RD, Ilkayeva O, Huang Z, Tollini LA, Murphy SK, et al. (2015). ACLY and ACC1 Regulate Hypoxia-Induced Apoptosis by Modulating ETV4 via alpha-ketoglutarate. PLoS Genet 11, e1005599. [PubMed: 26452058]

Kim MK, Osada T, Barry WT, Yang XY, Freedman JA, Tsamis KA, Datto M, Clary BM, Clay T, Morse MA, et al. (2012). Characterization of an oxaliplatin sensitivity predictor in a preclinical murine model of colorectal cancer. Molecular cancer therapeutics 11, 1500–1509. [PubMed: 22351745]

Laleu B, Gaggini F, Orchard M, Fioraso-Cartier L, Cagnon L, Houngninou-Molango S, Gradia A, Duboux G, Merlot C, Heitz F, et al. (2010). First in class, potent, and orally bioavailable NADPH oxidase isoform 4 (Nox4) inhibitors for the treatment of idiopathic pulmonary fibrosis. J Med Chem 53, 7715–7730. [PubMed: 20942471]

Lei QY, Zhang H, Zhao B, Zha ZY, Bai F, Pei XH, Zhao S, Xiong Y, and Guan KL (2008). TAZ promotes cell proliferation and epithelial-mesenchymal transition and is inhibited by the hippo pathway. Mol Cell Biol 28, 2426–2436. [PubMed: 18227151]

Lin L, Sabnis AJ, Chan E, Olivas V, Cade L, Pazarentzos E, Asthana S, Neel D, Yan JJ, Lu X, et al. (2015). The Hippo effector YAP promotes resistance to RAF- and MEK-targeted cancer therapies. Nat Genet 47, 250–256. [PubMed: 25665005]

Linkermann A, Skouta R, Himmerkus N, Mulay SR, Dewitz C, De Zen F, Prokai A, Zuchtriegel G, Krombach F, Welz PS, et al. (2014). Synchronized renal tubular cell death involves ferroptosis. Proc Natl Acad Sci U S A 111, 16836–16841. [PubMed: 25385600]

Medina-Rico M, Ramos HL, Lobo M, Romo J, and Prada JG (2018). Epidemiology of renal cancer in developing countries: Review of the literature. Canadian Urological Association Journal 12, E154. [PubMed: 29283089]

Mori M, Triboulet R, Mohseni M, Schlegelmilch K, Shrestha K, Camargo FD, and Gregory RI (2014). Hippo signaling regulates microprocessor and links cell-density-dependent miRNA biogenesis to cancer. Cell 156, 893–906. [PubMed: 24581491]

Panzilius E, Holstein F, Bannier-Hélaouët M, von Toerne C, Koenig A-C, Hauck SM, Ganz HM, Angeli JPF, Conrad M, and Scheel CH (2018). A cell-density dependent metabolic switch sensitizes breast cancer cells to ferroptosis. bioRxiv, 417949.

Park S, Ahn J-Y, Lim M-J, Kim M-H, Yun Y-S, Jeong G, and Song J-Y (2010). Sustained expression of NADPH oxidase 4 by p38 MAPK-Akt signaling potentiates radiation-induced differentiation of lung fibroblasts. Journal of molecular medicine 88, 807–816. [PubMed: 20396861]

Peng C, Zhu Y, Zhang W, Liao Q, Chen Y, Zhao X, Guo Q, Shen P, Zhen B, Qian X, et al. (2017). Regulation of the Hippo-YAP Pathway by Glucose Sensor O-GlcNAcylation. Mol Cell 68, 591–604 e595. [PubMed: 29100056]

Peng H, Li W, Seth DM, Nair AR, Francis J, and Feng Y (2013). (Pro) renin receptor mediates both angiotensin II-dependent and -independent oxidative stress in neuronal cells. PloS one 8, e58339. [PubMed: 23516464]

Perner A, Andresen L, Pedersen G, and Rask-Madsen J (2003). Superoxide production and expression of NAD(P)H oxidases by transformed and primary human colonic epithelial cells. Gut 52, 231–236. [PubMed: 12524405]

Poursaitidis I, Wang X, Crighton T, Labuschagne C, Mason D, Cramer SL, Triplett K, Roy R, Pardo OE, Seckl MJ, et al. (2017). Oncogene-Selective Sensitivity to Synchronous Cell Death following Modulation of the Amino Acid Nutrient Cystine. Cell Rep 18, 2547–2556. [PubMed: 28297659]

Schutte U, Bisht S, Heukamp LC, Kebschull M, Florin A, Haarmann J, Hoffmann P, Bendas G, Buettner R, Brossart P, et al. (2014). Hippo signaling mediates proliferation, invasiveness, and

metastatic potential of clear cell renal cell carcinoma. Transl Oncol 7, 309–321. [PubMed: 24913676]

Sedeek M, Nasrallah R, Touyz RM, and Hébert RL (2013). NADPH Oxidases, Reactive Oxygen Species, and the Kidney: Friend and Foe. Journal of the American Society of Nephrology 24, 1512–1518. [PubMed: 23970124]

Skouta R, Dixon SJ, Wang J, Dunn DE, Orman M, Shimada K, Rosenberg PA, Lo DC, Weinberg JM, and Linkermann A (2014). Ferrostatins inhibit oxidative lipid damage and cell death in diverse disease models. Journal of the American Chemical Society 136, 4551–4556. [PubMed: 24592866]

Sourbier C, Liao PJ, Ricketts CJ, Wei D, Yang Y, Baranes SM, Gibbs BK, Ohanjanian L, Spencer Krane L, Scroggins BT, et al. (2018). Targeting loss of the Hippo signaling pathway in NF2-deficient papillary kidney cancers. Oncotarget 9, 10723–10733. [PubMed: 29535838]

Stein C, Bardet AF, Roma G, Bergling S, Clay I, Ruchti A, Agarinis C, Schmelzle T, Bouwmeester T, Schübeler D, et al. (2015). YAP1 Exerts Its Transcriptional Control via TEAD-Mediated Activation of Enhancers. PLOS Genetics 11, e1005465. [PubMed: 26295846]

Tang X, Ding CK, Wu J, Sjol J, Wardell S, Spasojevic I, George D, McDonnell DP, Hsu DS, Chang JT, et al. (2017). Cystine addiction of triple-negative breast cancer associated with EMT augmented death signaling. Oncogene 36, 4379. [PubMed: 28604749]

Tang X, Wu J, Ding CK, Lu M, Keenan MM, Lin CC, Lin CA, Wang CC, George D, Hsu DS, et al. (2016). Cystine Deprivation Triggers Programmed Necrosis in VHL-Deficient Renal Cell Carcinomas. Cancer research 76, 1892–1903. [PubMed: 26833124]

Uronis JM, Osada T, McCall S, Yang XY, Mantyh C, Morse MA, Lyerly HK, Clary BM, and Hsu DS (2012). Histological and molecular evaluation of patient-derived colorectal cancer explants. PLoS One 7, e38422. [PubMed: 22675560]

Viswanathan VS, Ryan MJ, Dhruv HD, Gill S, Eichhoff OM, Seashore-Ludlow B, Kaffenberger SD, Eaton JK, Shimada K, Aguirre AJ, et al. (2017). Dependency of a therapy-resistant state of cancer cells on a lipid peroxidase pathway. Nature 547, 453–457. [PubMed: 28678785]

Walko G, Woodhouse S, Pisco AO, Rognoni E, Liakath-Ali K, Lichtenberger BM, Mishra A, Telerman SB, Viswanathan P, Logtenberg M, et al. (2017). A genome-wide screen identifies YAP/WBP2 interplay conferring growth advantage on human epidermal stem cells. Nature Communications 8, 14744.

Yang WS, SriRamaratnam R, Welsch ME, Shimada K, Skouta R, Viswanathan VS, Cheah JH, Clemons PA, Shamji AF, Clish CB, et al. (2014). Regulation of Ferroptotic Cancer Cell Death by GPX4. Cell 156, 317–331. [PubMed: 24439385]

Yang WS, and Stockwell BR (2016). Ferroptosis: Death by Lipid Peroxidation. Trends in Cell Biology 26, 165–176. [PubMed: 26653790]

Zanconato F, Cordenonsi M, and Piccolo S (2016). YAP/TAZ at the Roots of Cancer. Cancer Cell 29, 783–803. [PubMed: 27300434]

Zanconato F, Forcato M, Battilana G, Azzolin L, Quaranta E, Bodega B, Rosato A, Bicciato S, Cordenonsi M, and Piccolo S (2015). Genome-wide association between YAP/TAZ/TEAD and AP-1 at enhancers drives oncogenic growth. Nature cell biology 17, 1218. [PubMed: 26258633]

Zhang Q, Han X, Chen J, Xie X, Xu J, Zhao Y, Shen J, Hu L, Xu P, and Song H (2018). Yes-associated protein (YAP) and transcriptional coactivator with PDZ-binding motif (TAZ) mediate cell density–dependent proinflammatory responses. Journal of Biological Chemistry 293, 18071–18085. [PubMed: 30315101]

Zhao B, Wei X, Li W, Udan RS, Yang Q, Kim J, Xie J, Ikenoue T, Yu J, Li L, et al. (2007). Inactivation of YAP oncoprotein by the Hippo pathway is involved in cell contact inhibition and tissue growth control. Genes & Development 21, 2747–2761. [PubMed: 17974916]

Highlights

- Ferroptosis susceptibility can be affected by the cell density

- TAZ is activated in renal cell carcinoma cell lines and early-passage tumor cells

- The activation status of TAZ regulates the susceptibility of RCC to ferroptosis

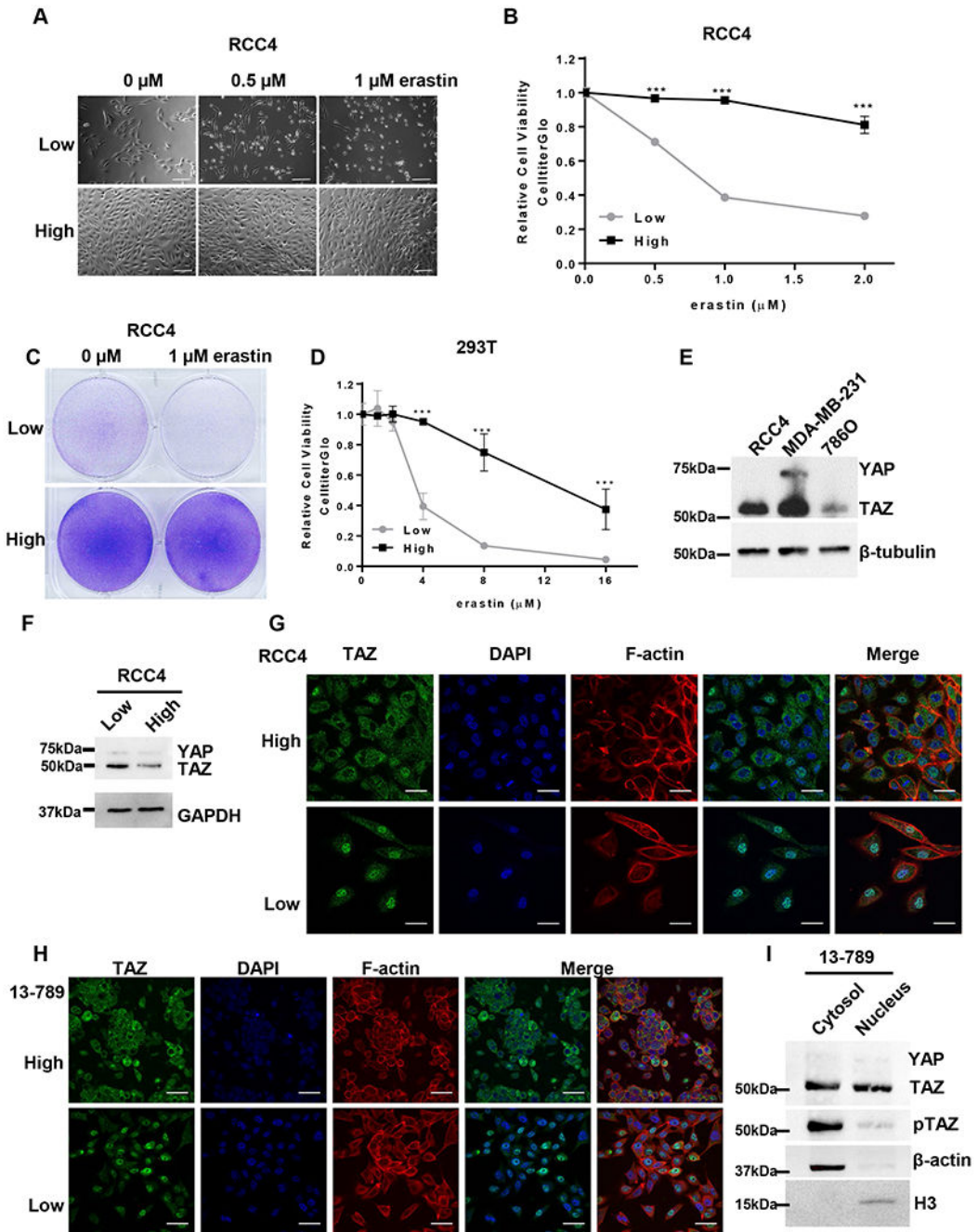- TAZ regulates ferroptosis through EMP1-NOX4 expression

Figure 1. Cell density regulates the sensitivity of RCC to the erastin-induced ferroptosis
(A) Bright field images of RCC4 cells cultured in low/high densities when treated with the indicated concentrations of erastin. Scale bar, 200 μm. (B) Cell viability assay by CelltiterGlo after RCC4 cells of low/high cell densities treated with indicated concentrations of erastin for 24 h. Data are represented as mean ± SEM from triplicate of one of four independent experiments (***p < 0.001). (C) Crystal violet staining of RCC4 cultured in low/high densities treated with vehicle or 1μM erastin. (D) Cell viability assay by CelltiterGlo after 293T cells grown at low vs. high (2500/10,000 cells per 96 well) cell

densities treated with indicated concentrations of erastin. Data are represented as mean ± SEM from triplicate of one of two independent experiments (***p < 0.001). (E) Western blot analysis of YAP and TAZ in renal carcinoma cell lines, RCC4 and 786-O cells, as well as in the breast cancer cell line, MDA-MB-231. Representative data of at least three independent experiments. (F) Western blot analysis of YAP and TAZ in RCC4 cells grown at low vs. high density. Representative data of at least two independent experiments. (G-H) Confocal immunofluorescence images of TAZ in RCC4 cells (G) or RCC PDX, 13-789, tumor cells (H) grown at low vs. high density. DAPI staining of cell nuclei and rhodamine-phalloidin staining for F actin cytoskeleton to mark cell boundaries. Merged images with nuclear stain, DAPI, are also shown. Scale bars, 50 μm.

(I) Western blot measuring YAP and TAZ abundance and phospho-TAZ (Ser89) in RCC PDX 13-789 cells of cytosolic/nucleic extractions. Histone H3 serves as a nuclear marker; β-actin serves as a cytosolic marker.
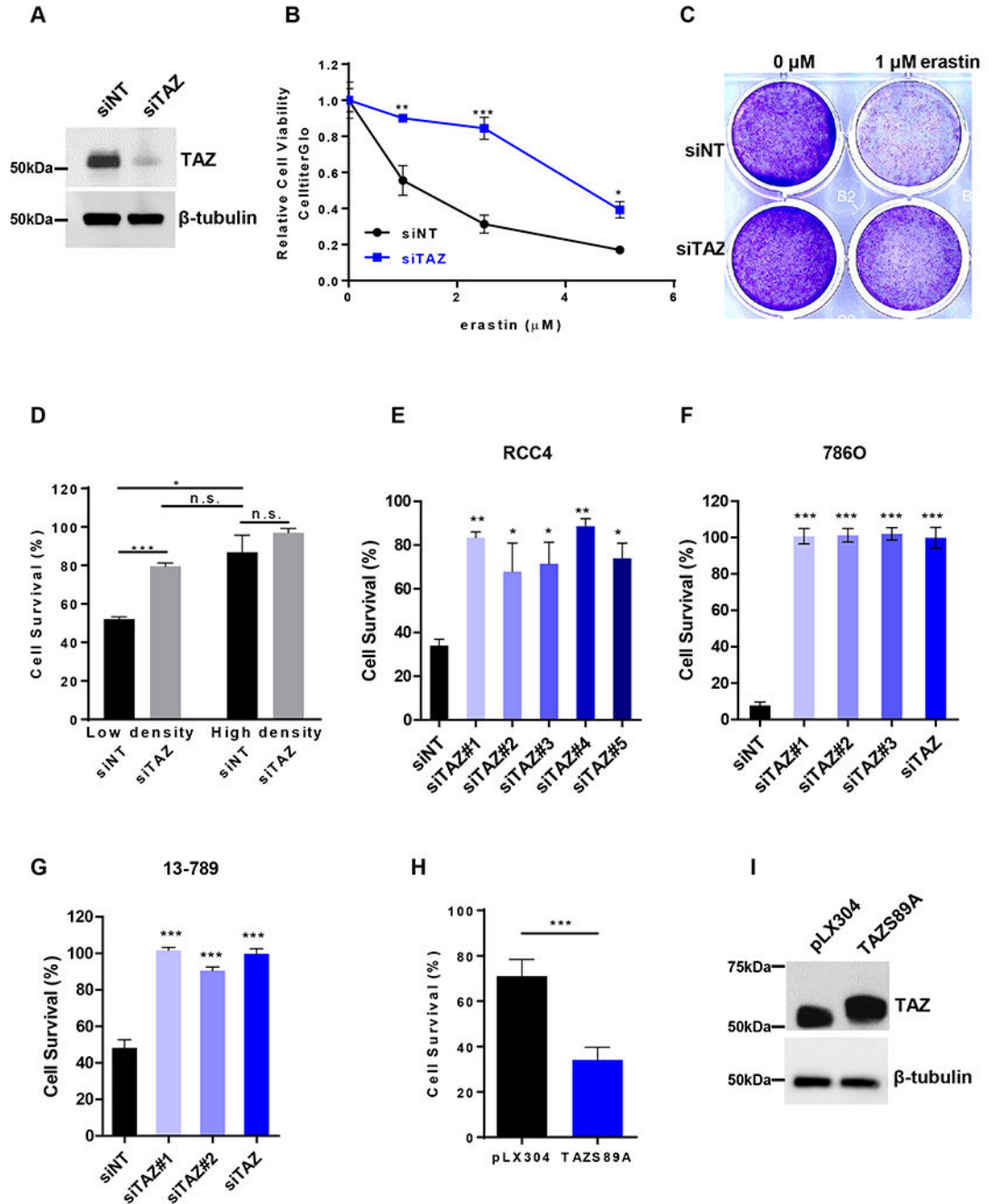
See also Figure S1.

Figure 2. TAZ regulates sensitivity to erastin-induced ferroptosis

(A-F) Silencing of TAZ reduces erastin-induced ferroptosis. RCC4 cells were treated with siRNA control, siNT, or siRNA targeting TAZ, siTAZ, for two days. (A) Cells were harvested for western blot analysis to check knockdown efficiency. (B) Cell viability was determined by CelltiterGlo after 24 hours of indicated dosage of erastin treatment. Data are represented as mean±SEM, n=3 (*p < 0.05; **p<0.01; ***p < 0.001). (C) Crystal violet staining of RCC4 treated with 1μM erastin for 2 days after incubating with siRNA control, siNT, or silencing of TAZ, siTAZ for 1 day. Representative data from one of two

independent studies. (D) RCC4 cells were treated with siRNA control, siNT, or siRNA targeting TAZ, siTAZ for 24 h. Later, cell viability was determined by CelltiterGlo after 24 h treatment of 1μM erastin. Data are represented as mean±SEM, n=3 by comparing to the DMSO controls of each group (*p < 0.05; ***p < 0.001, n.s : not significant). (E-G) Treatment of multiple individual siRNAs targeting TAZ (#1 to #5), siTAZ (pooled), or siRNA control, non-targeting (siNT) for two days in renal carcinoma cells, RCC4 cells (E), or 786O cells (F), or RCC PDX 13-789 cells (G). Cell viability was determined by CelltiterGlo after 24 h treatment of 2.5μM, 1μM and 16μM of erastin, respectively. Data are represented as mean±SEM, n=3 by comparing to the DMSO controls of each group (*p < 0.05; **p<0.01; ***p < 0.001).

(H-I) Overexpression of TAZ sensitizes RCC4 cells to erastin-induced ferroptosis. (H) RCC4 cells were transfected with pLX304 control vector or TAZS89A plasmid and then treated with 4μM erastin for 24 hours. Cell viability was then determined by CelltiterGo. Data are represented as mean±SEM, n=3 by comparing to the DMSO controls. (***p < 0.001) (I) Cells were also harvested for western blot analysis of TAZ.
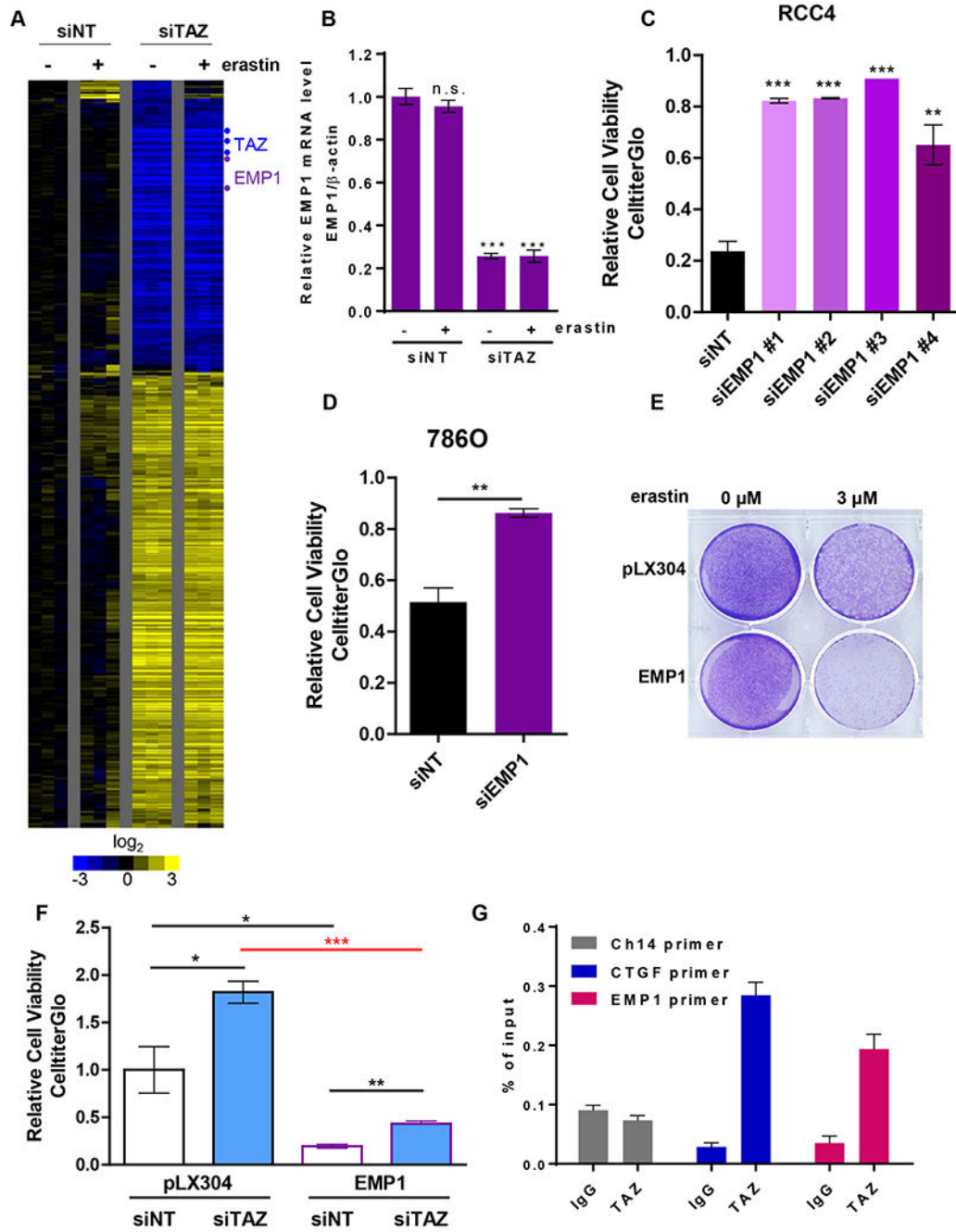
See also Figure S2.

Figure 3. EMP1 is a direct target gene of TAZ that regulates erastin-induced ferroptosis sensitivity

(A) Gene expression profiles were analyzed by U133A2.0 microarray in RCC4 cells after treating with 1µM erastin for 7 hours following silencing TAZ for two days.

(B) RT-qPCR validates that EMP1 is downregulated when TAZ is silenced by siRNAs. Data are represented as mean±SEM, n=3 after normalized to the DMSO controls (mock).

(C-D) siRNAs targeting EMP1 reduces erastin-induced ferroptosis. Treatment of siRNA control, non-targeting (siNT), multiple individual siRNAs targeting EMP1 (#1 to #4), or siEMP1 (pooled), for two days in renal carcinoma cells, RCC4 cells (C), or 786O cells

(D). Cell viability was determined by CelltiterGlo after 24 hours of 2μM and 1μM erastin, respectively. Data are represented as mean±SEM, n=3 by comparing to the DMSO controls.

(E) Overexpression EMP1 sensitizes RCC4 cells to ferroptosis. Crystal violet staining of RCC4 cells that are stably overexpress control vector, pLX304, or pLX304-EMP1-V5 (EMP1) after treating with 3μM erastin for 1 day.

(F) Genetic interaction between TAZ and EMP1. After stably overexpressing with EMP1, RCC4 cells were treated with siRNAs targeting TAZ. Later, cell viabilities were determined by CelltiterGlo after 24 hours of 2 μM erastin treatment. Data are represented as mean±SEM, n=3 after normalized to the DMSO controls (*p < 0.05; **p<0.01; ***p < 0.001).

(G) EMP1 is the direct target of TAZ. From RCC4 lysates, ChIP-qPCR with TAZ antibody (CST #70148) validates that TAZ binds to EMP1 promoter. ChIP-qPCR of the CTGF promoter serves as a positive control, while Ch14 serves as a negative control. Data from three technical replicates, mean±SEM, from one representative experiment out of four are shown.
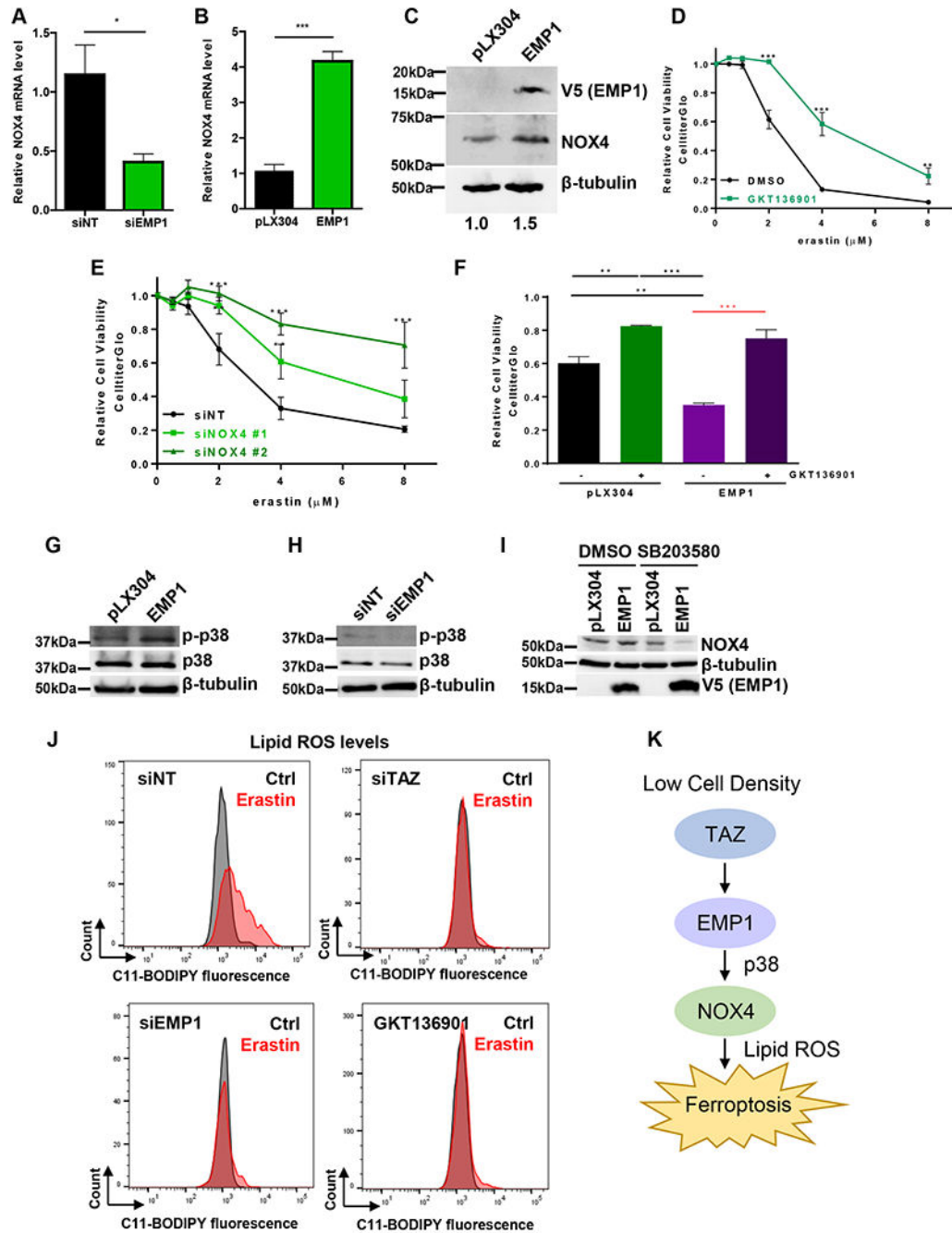
See also Figure S3.

Figure 4. EMP1 regulates ferroptosis through NOX4

(A) siRNA-mediated knockdown of EMP1 gene reduces the mRNA level of NOX4. Data are represented as mean ± SEM from triplicate of one of three independent experiments (*p < 0.05).

(B) Overexpression of EMP1 increases NOX4 mRNA level. Data are represented as mean ± SEM from triplicate of one of three independent experiments (***p < 0.001).

(C) Higher amount of NOX4 protein correlates with EMP1 overexpression. V5 antibody indicated EMP1-V5 overexpression. The western blots of NOX4 were quantified,

normalized to the β-tubulin, expressed relative to the control vector, and showed as below numbers. Representative data from one of at least three independent studies.

(D-E) Inhibition of NOX4 blocks erastin-induced ferroptosis. Cell viability was determined by CelltiterGlo after 24 hours of indicated concentrations of erastin with (D) NOX4 inhibitor, 10 μM GKT136901, mean±SEM, n=3, (E) silencing NOX4 by two individual siRNAs. mean±SEM, n=7, Data are represented by comparing to the DMSO controls (**p<0.01; ***p < 0.001).

(F) Genetic interaction between EMP1 and NOX4. Cell viabilities were determined by CelltiterGlo after RCC4 cells were treated with EMP1 overexpression for 1 day following 20 μM NOX4 inhibitor, GKT136901 and 8 μM erastin for 1 day. Data are represented as mean±SEM, n=3 after normalized to the DMSO controls.

(G-H) Western blot analysis of phospho-p38 (Thr180/Tyr182), total p38, and control β-tubulin upon overexpression of EMP1 (G) or siRNA-mediated silencing of EMP1 (H).

(I) Western blot analysis of NOX4 upon overexpression of EMP1 with treatment of p38 inhibitor, SB203580.

(J) Inhibition of TAZ, EMP1, or NOX4 abolishes elevated lipid-ROS by erastin treatment. Lipid ROS in RCC4 cells treated with knockdown TAZ or EMP1 as well as inhibition of NOX4 was assessed by flow cytometry using C11-BODIPY. Representative data from one of five independent studies.

(K) A schematic model illustrating the erastin-induced ferroptosis regulated by TAZ-EMP1-NOX4 axis.

See also Figure S4.